The carbonate pathway for formation of manganese enrichments in reducing environments

Authors: Chad Wittkop, Elizabeth D. Swanner, Ashley Grengs, Nicholas Lambrecht, Mojtaba Fakhraee, Amy Myrbo, Andrew W. Bray, Simon W. Poulton, and Sergei Katsev

Supplementary Materials

S1. Study site

Brownie Lake (BL) is a small ferruginous kettle lake located in Minneapolis, Minnesota (N44.9676° W93.3245°; figure S1). Historical and paleolimnologic analysis suggests that BL has been meromictic since 1917, when its surface elevation was lowered by construction of a canal joining it with adjacent Cedar Lake (Swain, 1984; Tracey et al., 1996). Profundal sediments are continuously laminated above this horizon, and laminations are annual (Swain, 1984). BL surface area is 4.0 ha (compared to 13.2 ha pre-1917), and its max depth is now 14 m (compared to an estimated 17 m). The lake's reduced surface area and fetch, and surface elevation low in its basin, have reduced its susceptibility to wind entrainment of surface waters and vertical water column mixing. An industrial cooling water outlet also contributed to increased concentrations of dissolved Fe^{2+}, alkalinity, and SiO_2 in the late 20th century (Swain, 1984), and contamination from road salt has further increased total salinity and stability of the water column (Novonty et al., 2008; Myrbo et al., 2011; Lambrecht et al., 2018). Isolation of the cold (7°C) lake bottom waters from atmospheric O_2 resupply, along with a high flux of algal and terrestrial organic carbon, have driven evolution to low Eh and pH conditions, under which minerals such as iron (hydr)oxides and carbonates may dissolve, increasing bottom water density and strengthening stratification. The persistent, stable nature of the stratification is particularly evident in repeated monitoring of water column conductivity (Lambrecht et al. 2018).

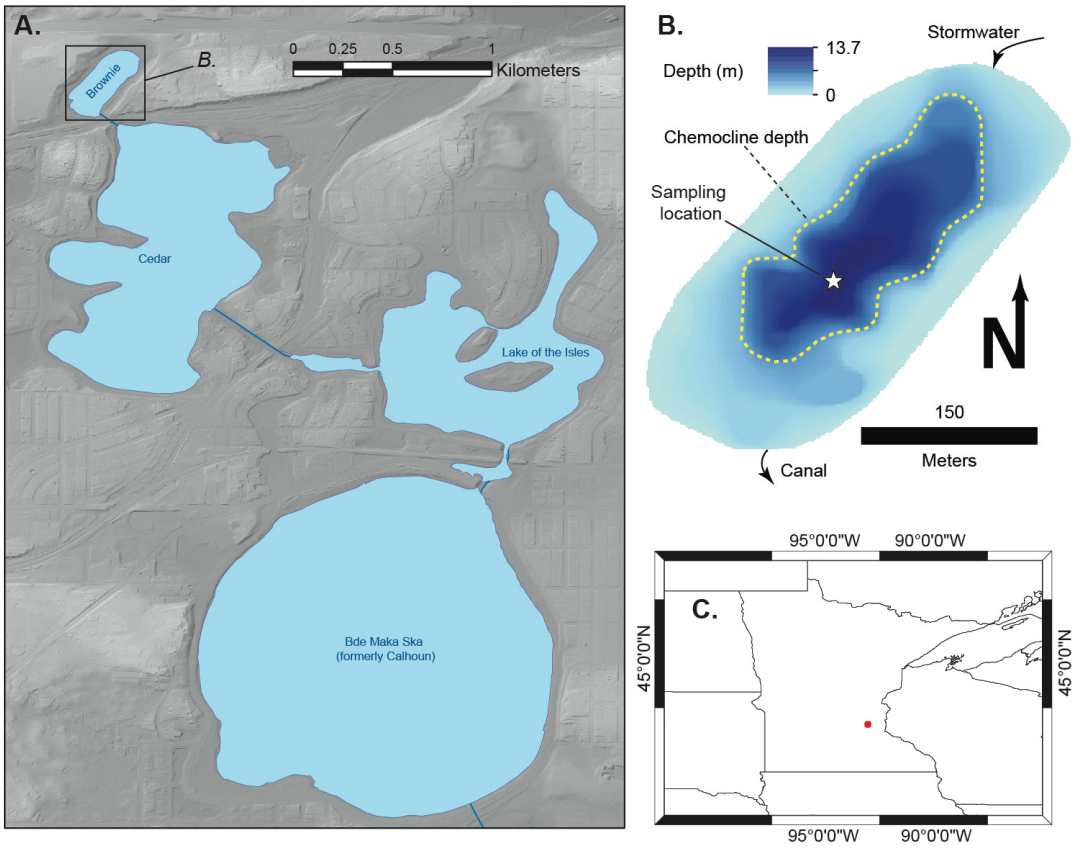

Figure S1: A. Location of Brownie Lake relative to the Minneapolis Chain of Lakes. B. Brownie Lake bathymetry showing sampling location and approximate area of anoxic zone. C. Location in Minnesota, USA.

S2. Methods

Methods employed in water column analysis in BL are described in detail by Lambrecht et al. 2018 and Lambrecht et al. in 2020. We review key approaches here.

S2.1 Water column profiles

Water column properties at BL were monitored using in situ sensors for dissolved oxygen, temperature, conductivity, and pH with either a Hydrolab DS-5 sonde or a YSI ProDSS. All sensors were calibrated according to the manufacturer's specifications.

S2.2. Water samples

Water samples were collected from direct pumping for smaller samples, or a Van-Dorn type opaque, non-metallic sampler for samples requiring larger volumes. Pumped samples were collected from polypropylene or Tygon tubing, and immediately filtered in the field with a filter connected to tubing to minimize exposure to O_2. Samples for cations, anions, and dissolved carbon (DIC, CH_4) analysis were filtered at 0.45 μm. Cation samples were preserved with HNO_3, and CH_4 samples were preserved with HCl or kept cool prior to analysis.

Cations were analyzed by ICP-OES at the University of Minnesota Department of Earth Sciences (2015 samples), or the U of MN Research Analytical Laboratory (2017-2018 samples). Anions were analyzed at the same facilities using an ion chromatograph. Samples for determining total sulfide were stored on ice or at 4°C until laboratory analysis could be completed, usually within 72 hours, and analyzed by Cline assay (detection limit: 1 μM; Cline, 1969; Reese et al., 2011) and measured spectrophotometrically on an Epoch 2 Microplate Reader (Biotek). Nitrate and ammonium samples were analyzed spectrophotometrically as described by Lambrecht et al., 2018.

Mineral saturation indices were calculated using Geochemist's Workbench (Bethke, 1996) incorporating cation-anion data, DIC, and sonde measurements of O_2 (O_2 measurements were entered as zero values below the detection limit of the sonde, usually 2-3 μM) and pH. Pseudokutnahorite saturation was calculated using Ca^{2+}, Mn^{2+}, and CO_3^{2-} activities calculated in Visual Minteq 3.1 (https://vminteq.lwr.kth.se) and the solubility constant of Mucci (1991).

Concentration of dissolved inorganic carbon (DIC) was determined by measuring the CO_2 concentration of gas evolved from a 1 mL water sample injected with 1 mL of 85% phosphoric acid using a GasBench II system. The $\delta^{13}C$ of DIC was measured from the same evolved gas sample at the UC Davis Stable Isotope Facility (UCDSIF) a Delta V Plus IRMS (Thermo Scientific, Bremen, Germany) coupled to the GasBench II. Final

$\delta^{13}C$ values are expressed relative to the international standard V-PDB (Vienna PeeDee Belemnite) with long term standard deviation of DIC analyses is 0.1 ‰.

Stable isotope ratios of dissolved methane carbon ($\delta^{13}C$) were measured at UCDSIF using a ThermoScientific Precon concentration unit interfaced to a ThermoScientific Delta V Plus isotope ratio mass spectrometer (ThermoScientific, Bremen, Germany). Gas samples are scrubbed of H_2O / CO_2 and CH_4 is separated from residual gases by a GS-CarbonPLOT GC column. Purified CH_4 is oxidized to CO_2 and analyzed by IRMS. Standards are calibrated against NIST 8559, 8560, and 8561 and final δ-values, are expressed relative to the international standards V-PDB (Vienna PeeDee Belemnite) with long-term standard deviation of 0.2 ‰.

S2.3. Particulates and sediments

Water column particulate samples were collected in August 2018 by direct pumping of BL water through Tygon tubing onto pre-weighed polycarbonate 0.2 μM filters in reusable polycarbonate housings from indicated depths until the filters became clogged. Inlet and outlet hoses were then clamped to prevent oxygen contact, and collected samples were immediately transferred into an N_2-filled glove bag for removal from the filter housing and storage and transport in an N_2-filled airtight container with Oxoid™ AnaeroGen™ sachets (TermoScientific).

Surface sediment samples were also collected from BL in August 2018 using an Aquatic Research Instruments gravity coring device. The top 1 cm of sediment was extruded from the corer and immediately transferred to N_2-flushed 100 mL glass septum bottles, stoppered with butyl rubber and crimped closed with aluminum caps.

Water column sediment traps were deployed in BL from June through October 2018. Traps consisted of a 0.5-m polycarbonate tube of 2-inch diameter attached to a 1-L Nalgene bottle. During recovery traps were immediately transferred into an N_2-filled glove bag and trapped material transferred into large glass vials with butyl stoppers, and subsequently stored in an anoxic glove box at Iowa State University.

Filter particulates, sediment trap materials, and sediment samples were freeze-dried. Mn was extracted from 50-100 mg of material using 10 mL of 0.5 M HCl for 1

hour (Thamdrup et al., 1994). This extraction, used as part of the modified Fe sequential extraction (Xiong et al., 2019) developed by Poulton and Canfield (2005), targets solid phase Mn^{2+}, and Mn carbonates, but only targets Mn-oxides if a reductant is present (Thamdrup et al., 1994). Total Mn was determined following total digestion of the freeze-dried samples by ashing at 550 °C followed by dissolution in HNO_3-HF-$HClO_4$ and evaporation to dryness. Boric acid was added to the residue (to dissolve aluminium hexafluoride) and evaporated to dryness, before redissolution in 50% HCl. Mn in the extractants were quantified by AAS (Thermo Scientific iCE3000 series) with RSD not exceeding 2.1%.

S2.4 X-ray diffraction

Surface sample bulk mineralogy was assessed by powder X-ray diffraction. Samples were gently homogenized in a cleaned agate mortar and loosely packed into an aluminum target for analysis on a Rigaku Ultima-IV with Cu-Kα radiation scanned from 5-75° 2θ with a 0.02° step size with an X-ray energy of 44 kV and 40 mA. Counts were measured with a D/Tex detector which allows for a scan speed of 6° per minute.

The sediment trap sample, homogenized as above, was analyzed at Iowa State University on a Siemens D500 diffractometer using Cu-Kα radiation at 45kV and 30mA from 4-75° 2θ with a 0.05° step size and a scan rate of 2° per minute.

S2.5 Geochemical modeling

Brownie Lake cation, anion, DIC, pH, and O_2 data were imported to Geochemist's Workbench (GWB; version 8.0.12 build 4427; Bethke, 1996) to assess the sensitivity of carbonate mineral saturation to processes occurring near a ferruginous chemocline. Activity coefficients were modeled utilizing the standard “B-dot” or extended Debye-Huckel equation, which is valid in solutions with ionic strengths up to 3 molal (Bethke and Yeakel, 2010); the maximum ionic strength of solutions we modeled was ~0.66 molal. Processes we considered included included photoferrotrophy (as discussed in Crowe et al., 2008), methanotrophy (Lambrecht et al., 2020), and sulfate reduction

(Walter et al., 2014), in addition to processes that would be implicated in typical temperate lake water columns including calcite dissolution and organic carbon respiration (Myrbo and Shapley, 2006). To simplify our approach, we focused these efforts on three primary carbonates: calcite, rhodochrosite, and siderite, though precursor metastable carbonates likely play a role in these processes (e.g. Mucci, 1991; Jiang and Tosca, 2019; Vuillemin et al., 2019). We also focus on calcite rather than aragonite as the former is the primary phase in most freshwater lakes (e.g. Thompson et al., 1997), and recent experiments demonstrate that the calcite lattice is more accommodating of Mn incorporation than is aragonite (Son et al. 2019).

To assess changes to mineral saturation and precipitation we ran scenarios in both unsuppressed (minerals allowed to precipitate at saturation) and suppressed (mineral precipitation blocked) conditions. Although the assumption that minerals would precipitate at saturation is largely unrealistic (siderite in particular may require multi-fold oversaturation, e.g. Jiang and Tosca, 2019; Vuillemin et al., 2019), this view of the system is useful in assessing the ratios of minerals that could be produced by these waters.

In simulations where calcite was added, the rate of addition was tied to the concentration of calcite that was generated in an unsuppressed simulation with Brownie Lake surface water chemistry of July 2017 (surface water calcite abundance at equilibrium 115.6 μmol with dolomite minerals suppressed) and divided over the 15 day simulation (7.7 μmol calcite added per day). The length of the simulation was selected on the basis of the duration of whiting events (days to weeks, e.g. Shinn et al., 1989; Thompson et al., 1997) as well as seasonal changes observed between mid- and late summer in the Brownie Lake water column manifested in the upward migration of the oxycline (e.g. Lambrecht et al., 2018, discussion below). Simulations with longer reaction times did not change the fundamental results, which were governed by initial conditions and selection of reaction rates. These rates were determined based on dividing initial concentrations of reactants measured in the water column (e.g. O_2, SO_4) by a 15-day model simulation.

An initial series of simulations assessed sensitivity of carbonate saturation to the following processes: calcite addition, CO_2 addition, CO_2 removal, and sulfate reduction.

Aerobic respiration (AR) and CH_4 oxidation (MO) were tracked using the following stoichiometries:

(S1) $CH_2O + O_2 = CO_2 + H_2O$

(S2) $CH_4 + 2O_2 = CO_2 + 2H_2O$

With the key differences being the ratio of O_2 removed to CO_2 added: 2:1 for MO, and 1:1 for AR.

Sulfate reduction (SR) was simulated using the following stoichiometry:

(S3) $SO_4^{2-} + 2CH_2O = H_2S + 2HCO_3^-$

In all of the cases above the concentrations of CH_4 and CH_2O were assumed to be unlimited relative to the concentration of electron acceptors. The impacts of oxygenic photosynthesis and photoferrotrophy were also assessed but found to have negligible influence given the low light availability. The three intervals selected for detailed modeling based on initial simulation each showed greater sensitivity to changes in Mn-carbonate saturation relative to others.

S3. Supplemental Results and Discussion

S3.1 Phosphorus cycling in Brownie Lake

A $Mn(II)HPO_4$ phase becomes saturated at the chemocline, along with vivianite ($Fe^{2+}_3(PO_4)_2 \cdot 8H_2O$; Figure S2). Both phosphate phases achieve maximum saturation in deep water at 13 m depth (max SI = 0.54 for vivianite, max SI = 3.50 for $MnHPO_4$). The reliability of the solubility product of the Mn-PO_4 phase has been questioned (Schwab, 1989), hence we focus discussion in the main text on carbonate phases. However, additional discussion of P-phases in ferruginous environments is warranted here.

Phosphate phases are a significant particulate shuttle for Fe in ferruginous lakes (Cosmidis et al., 2014), and may also play a role in the ferruginous Mn cycle. Mn is recognized to substitute for Fe in diagenetic vivianite in both freshwater and marine examples (Postma, 1981; Nakano, 1992; Friedl et al., 1997; Egger et al., 2015). Vivianite and Mn-PO_4 phases are identified components in the particulate load from ferruginous Lac Pavin (Cosmidis et al., 2014; Miot et al., 2016; Rivas-Lamelo et al., 2017), with vivianite representing a dominant particulate component in deep waters.

However, these phosphate phases are not detectable in surface sediment XRD (main text). Vivianite may indeed be a component in BL sediments, but it does not appear to play as large a role as calcite. Detailed assessments of phosphorus cycling in Brownie Lake are the focus of ongoing work.

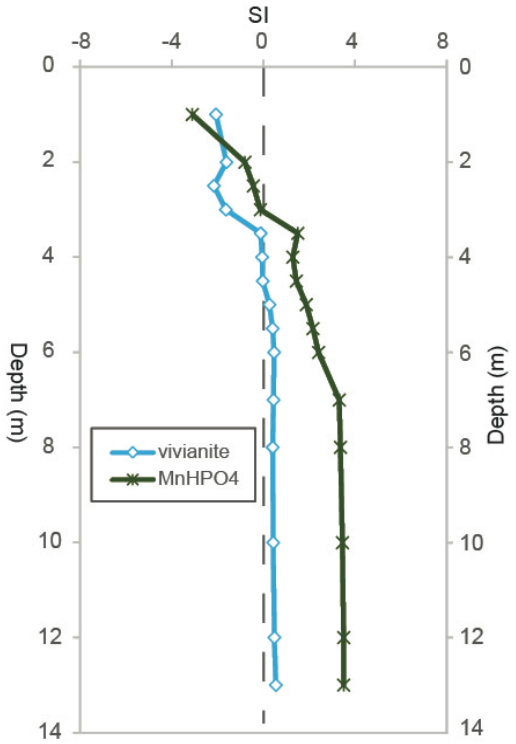

Figure S2: Solubility index (SI) of phosphate phases in Brownie Lake, July 2017.

S3.2 Brownie Lake DIC mass balance analysis

We employed a mass balance to determine the degree to which SR and MO may contribute to the $\delta^{13}C_{DIC}$ excursion at the chemocline in BL. Using September 2017 data (where the largest isotope excursion was observed), we consider the influence on DIC composition from the equations S1-S3 above, which were rebalanced in terms of bicarbonate:

(S4) $CH_2O + O_2 = HCO_3^- + H^+$

(S5) $SO_4^{2-} + 2CH_2O = 2HCO_3^- + H_2S$

(S6) $CH_4 + 3/2O_2 = HCO_3^- + 3H^+$

Pathways S4 and S6 produce acidity, while pathway S5 leads to accumulation of bicarbonate. Iron and manganese reduction may additionally contribute to methane and organic carbon oxidation in this zone as discussed in 4.1 of the main text, but we will focus the following discussion on these three pathways illustrated above as they are the best constrained by presently available data.

By assuming that the bulk of the $\delta^{13}C_{DIC}$ shift across the oxycline (from -9.88‰ at 3 m to -11.98‰ at 4 m) is attributable to aerobic respiration, we can evaluate the relative influence of SR and MO on the remaining depletion to a minimum value of -12.87‰ observed at 5 m. At this depth, 25 μM of sulfide was measured, which would account for an additional 50 μM of bicarbonate at a $\delta^{13}C$ of ~-30‰ (an estimate for the composition of organic carbon, e.g. Havig et al. 2017). This would shift $\delta^{13}C_{DIC}$ to -12.32‰, or 0.5‰ higher than the observed value. Oxidizing an additional 29 μM of methane (assuming a $\delta^{13}C$ of -64‰ for CH_4) would shift DIC to the observed carbon isotopic composition, but not its observed concentration. We account for the sharp increase in the concentration of DIC at the chemocline by mixing with DIC at the $\delta^{13}C$ composition of water at 5.5 m depth (-11.85‰), requiring 50 μM of methane to be oxidized (in addition to sulfate reduction) to counteract the influence of the large DIC concentration increase, or a total

of 79 μM of methane against 25 μM of SO_4, or a ratio of ~3:1 MO:SR. Limiting MO to only the cumulative concentration of dissolved O_2 observed between 4-5 m (26.6 μM), would oxidize 17.7 μM of CH_4, which would shift $\delta^{13}C$ to -12.43‰ against the total DIC reservoir.

These scenarios represent only a lower limit on the influence of SR and MO on $\delta^{13}C_{DIC}$ at the BL chemocline as we react only a residual amount of oxygen measured in the water column: additional CH_4 and SO_4 could have reacted, and iron-sulfide burial in particular may mask the true scale of SR in these waters.

S3.3 Thermodynamic calculations

Table S1 displays Gibbs Free Energy (ΔG_{rxn}) and redox potential of key reactions discussed in the main text, as calculated from conditions measured in BL waters.

Reaction	ΔG_{rxn} (kJ/mol)	E (V)
$CH_4 + 2\ O_2 = HCO_3^- + H^+ + H_2O$	-815.2	-
$HS^- + 2\ O_2 = SO_4^{2-} + H^+$	-764.8	-
$Fe^{2+} + 0.25\ O_2 + 2.5\ H_2O = Fe(OH)_3 + 2\ H^+$	-64.99	-
$Mn^{2+} + 0.5\ O_2 + H_2O$ = Pyrolusite + $2\ H^+$	-51.65	-
Half-reaction		
$CH_{4(aq)} + 3\ H_2O = HCO_3^- + 9\ H^+ + 8\ e^-$	-	0.202
$H_2S_{(aq)} + 4\ H_2O = SO_4^{2-} + 10\ H^+ + 8\ e^-$	-	0.290
$Fe^{2+} + 3\ H_2O = Fe(OH)_3 + 3\ H^+ + e^-$	-	1.060
$Mn^{2+} + 2\ H_2O$ = Pyrolusite + $4\ H^+ + 2\ e^-$	-	1.228

Table S1: Calculated ΔG_{rxn} and E for key reactions discussed in text. All calculated based on BL conditions in July 2017 6 m at temperature 7.6 °C (Table 1) except reactions involving sulfide, which were calculated from September 2017 data at 5 m and a temperature of 15.1 °C.

Supplementary References

Bethke, C., 1996. Geochemical reaction modeling: concepts and applications. Oxford UP, 397 p.

Bethke, C. M., and Yeakel, S., 2010. The Geochemist's Workbench Release 8.0 GWB Essentials Guide. RockWare, 122 p.

Busigny, V., Jezequel, D., Cosmidis, J., Viollier, E., Benzerara, K., Planavsky, N.J., Alberic, P., Lebeau, O., Sarazin, G., and Michard, G., 2016. The iron wheel in Lac Pavin: Interaction with the phosphorous cycle. In: Sime-Ngano et al. (Eds.), Lake Pavin, Springer International, p. 205-220.

Cline, J. D., 1969. SPECTROPHOTOMETRIC DETERMINATION OF HYDROGEN SULFIDE IN NATURAL WATERS. Limnology and Oceanography, v. 14, p. 454–458.

Cosmidis, J., Benzerara, K., Morin, G., Busigny, V., Lebeau, O., Jezequel, D., Noel, V., Dublet, G., and Othmane, G., 2014, Biomineralization of iron phosphates in the water column of Lake Pavin (Massif Central, France): Geochimica Cosmochimica Acta, v. 126, p. 78-96.

Crowe, S.A., Jones, C., Katsev, S., Magen, C., O'Neil, A.H., Sturm, A., Canfield, D.E., Haffner, G.D., Mucci, A., Sundby, B., and Fowle, D.A., 2008. Photoferrotrophs thrive in Archean ocean analogue. Proceedings of the National Academy of Sciences, v. 105, p. 15938-15943.

Crowe, S., Katsev, S., Leslie, K., Sturm, A., Magen, C., Nomosatryo, S., Pack, M., Kessler, J., Reeburgh, W., and Roberts, J., 2011, The methane cycle in ferruginous Lake Matano: Geobiology, v. 9, no. 1, p. 61-78.

Egger, M., Jilbert, T., Behrends, T., Rivard, C., and Slomp, C.P., 2015. Vivianite is a major sink for phosphorus in methanogenic coastal surface sediments. Geochimica Cosmochimica Acta, v. 169, p. 217-235.

Friedl, G., Wehrli, B., and Manceau, A., 1997. Solid phases in the cycling of manganese in eutrophic lakes: New insights from EXAFS spectroscopy. Geochimica Cosmochimica Acta, v. 61, p. 275-290.

Jiang, C.Z., and Tosca, N.J., 2019. Fe(II)-carbonate precipitation kinetics and the chemistry of anoxic ferruginous seawater. Earth and Planetary Science Letters, v. 506, p. 231-242.

Lambrecht, N., Wittkop, C., Katsev, S., Fakhraee, M., and Swanner, E.D. Geochemical characterization of two ferruginous meromictic lakes in the Upper Midwest, USA, 2018. Journal of Geophysical Research – Biogeosciences, doi:10.1029/2018JG004587.

Lambrecht, N., Katsev, S., Wittkop, C., Hall, S.J., Sheik, C.S., Picard, A., Fakhraee, M., and Swanner, E.D., 2020. Biogeochemical and physical controls on methane fluxes from two ferruginous meromictic lakes. Geobiology, v. 18, p. 54-69, doi: 10.1111/gbi.12365.

Miot, J., Jezequel, D., Benzerara, K., Cordier, L., Rivas-Lamelo, S., Skouri-Panet, F., Ferard, C., Poinsot, M., and Dupart, E., 2016. Mineralogical diversity in Lake Pavin: Connections with water column chemistry and biomineralization processes. Minerals, v. 6., doi:10.3390/min6020024.

Mucci, A., 1991. The solubility and free energy of formation of natural kutnahorite. Canadian Mineralogist, v. 29., p. 113-121.

Myrbo, A., and Shapley, M., 2006, Seasonal water-column dynamics of dissolved inorganic carbon stable isotopic compositions ($\delta^{13}C_{DIC}$) in small hardwater lakes in Minnesota and Montana: Geochimica et Cosmochimica Acta, v. 70, no. 11, p. 2699-2714.

Myrbo, A., Murphy, M., and Stanley, V., 2011. The Minneapolis Chain of Lakes by bicycle: Glacial history, human modifications, and paleolimnology of an urban natural environment. In Miller, J.D., Hudak, G.J., Wittkop, C., and McLaughlin, P.I., eds., Archean to Anthropocene: Field Guides to the Geology of the Mid-Continent of North America, Geological Society of America Field Guides 24, 425-437.

Nakano, S., 1992. Manganoan vivianite in the bottom sediments of Lake Biwa, Japan. Mineralogical Journal, v. 16, p. 96-107.

Novonty, E.V., Murphy, D., and Stefan, H.G., 2008. Increase of urban lake salinity by road deicing salt. Science of the Total Environment, v. 406, p, 131-144.

Postma, D., 1981. Formation of siderite and vivianite and the pore-water composition of a recent bog sediment in Denmark. Chemical Geology, v. 31, p. 225-244.

Poulton, S.W., and Canfield, D.E., 2005. Development of a sequential extraction procedure for iron: implications for iron partitioning in continentally derived particulates. Chemical Geology, v. 214, p. 209-221.

Reese, B.K., Finneran, D.W., Mills, H.J., Zhu, M.-X. and Morse, J. W., 2011. Examination and Refinement of the Determination of Aqueous Hydrogen Sulfide by the Methylene Blue Method. Aquatic Geochemistry, v. 17, p. 567–582.

Rivas-Lamelo, S., Benzerara, K., Lefevre, C.T., Montiel, C.L., Jezequel, D., Menguy, N., Viollier, E., Guyot, F., Ferard, C., Poinsot, M., Skouri-Panet, F., Trcera, N., Miot, J., and Dupart, E., 2017. Magnetotactic bacteria as a new model for P sequestration in the ferruginous Lake Pavin. Geochemical Perspectives Letters, v. 5., doi:10.7185/geochemlet.1743.

Scholz, C., Talbot, M., Brown, E., and Lyons, R., 2011. Lithostratigraphy, physical properties and organic matter variability in Lake Malawi Drillcore sediments over the past 145,000 years: Palaeogeography, Palaeoclimatology, Palaeoecology, v. 303, no. 1, p. 38-50.

Schwab, A.P., 1991. Manganese-phosphate solubility relationships in an acid soil. Soil Science Society of America Journal, v. 53, p, 1654-1660.

Shinn, E.A., Steinen, R.P., Lidz, B.H., and Swart, P.K., 1989. Whitings, a sedimentologic dilemma. Journal of Sedimentary Petrology, v. 59, p. 147-161.

Son, S., Newton, A.G., Jo, K., Lee, J-Y., and Kwon, K.D., 2019. Manganese speciation in Mn-rich $CaCO_3$: A density functional theory study. Geochimica et Cosmochimica Acta, v. 248, p. 231-241.

Swain, E.B., 1984, The paucity of blue-green algae in meromictic Brownie Lake: iron-limitation or heavy-metal toxicity [Ph.D. thesis]: Minneapolis, University of Minnesota, 362 p.

Thamdrup, B., Fossing, H., and Jørgensen, B.B., 1994. Manganese, iron and sulfur cycling in a coastal marine sediment, Aarhus bay, Denmark. Geochimica et Cosmochimica Acta, v. 58, p. 5115-5129.

Thompson, J.B., Schultze-Lam, S., Beveridge, T.J., and Des Marais, D.J., 1997. Whiting events: Biogenic origin due to the photosynthetic activity of cyanobacterial picoplankton. Limnology and Oceanography, v. 42, p. 133-141.

Tracey, B., Lee, N., and Card, V., 1996. Sediment indicators of meromixis: comparison of laminations, diatoms, and sediment chemistry in Brownie Lake, Minneapolis, USA. Journal of Paleolimnology v. 15, p. 129-132.

Vuillemin, A., et al., 2019. Formation of diagenetic siderite in modern ferruginous sediments. Geology, v. 47, p. 540-544.

Xiong, Y., Guilbaud, R., Peacock, C.L., Cox, R.P., Canfield, D.E., Krom, M.D., and Poulton, S.W., 2019. Phosphorus cycling in Lake Cadagno, Switzerland: A low sulfate euxinic ocean analogue. Geochimica et Cosmochimica Acta, v. 251, p. 116-135.

Walter, X.A., Picazo, A., Miracle, M.R., Vicente, E., Camacho, A., Aragno, M., and Zopfi, J., 2014. Phototrophic Fe(II)-oxidation in the chemocline of a ferruginous meromictic lake. Frontiers in Microbiology, doi: 10.3389/fmicb.2014.00713.